High-Pressure Chemistry | Hot Paper

DOI: 10.1002/ange.201308682

Observing High-Pressure Chemistry in Graphene Bubbles**

*Candy Haley Yi Xuan Lim, Milos Nesladek, and Kian Ping Loh**

Abstract: *Using IR spectroscopy, high-pressure reactions of molecules were observed in liquids entrapped by graphene nanobubbles formed at the graphene–diamond interface. Nanobubbles formed on graphene as a result of thermally induced bonding of its edges with diamond are highly impermeable, thus providing a good sealing of solvents within. Owing to the optical transparency of graphene and diamond, high-pressure chemical reactions within the bubbles can be probed with vibrational spectroscopy. By monitoring the conformational changes of pressure-sensitive molecules, the pressure within the nanobubble can be calibrated as a function of temperature and it is about 1 GPa at 600 K. The polymerization of buckministerfullerene (C_{60}), which is symmetrically forbidden under ambient conditions, is observed to proceed in well-defined stages in the pressurized nanobubbles.*

Graphene is a unique two-dimensional electron system as well as the thinnest elastic membrane found in nature. A consequence of graphene being a soft membrane is that it can be strain-enginneered to form ripples or bubbles. The impermeablity of graphene as well as its huge elastic modulus[1] suggests that these bubbles can be used as a barrier for entrapping fluids, forming a liquid cell. Yuk et al. applied the graphene membrane as sealing windows to trap liquids and used transmission electron microscopy to study the in situ growth of nanocrystals in it.[2] We have previously demonstrated that graphene–diamond interface undergoes bonding at high-temperature to transform the graphene into an undulating sheet of graphene nanobubbles (GNB) on the diamond substrate. Interfacial stress and rippling of graphene on the lattice-mismatched diamond produce a high density of nanometer-sized GNB on its surface. When heated to high temperatures, the entrapped water within the GNB can be transformed into the supercritical phase.[3] It is interesting to consider whether we can make use of the optical transparency of diamond and graphene to monitor high-pressure–high-temperature reactions inside the GNB. We encapsulated organic fluids inside a random array of GNBs that were formed by thermally annealing the graphene–diamond interface to the reconstruction temperature of diamond. One question is how do we probe the pressure inside these bubbles when they are heated? The probing of pressure in a nanosized bubble is non-trivial because using conventional methods such as ruby luminescence will be difficult.[4]

The strategy we applied herein is to entrap pressure-sensitive molecules such as polyphenyl molecules inside the bubble and follow its pressure-induced conformational change using an IR spectroscopic probe. Furthermore, to test the feasibility of graphene bubbles as a high-pressure anvil, polymerization of buckminsterfullerene (C_{60}) was tested within these nanobubbles, as its intermolecular coupling by cycloaddition reactions is symmetry-forbidden under normal conditions.

Transfer of CVD graphene onto diamond substrate was accomplished using the conventional float-transfer technique (see the Supporting Information for Raman characterization). Owing to surface tension at the air–water interface, graphene film floating on the air–water boundary becomes rippled and entraps water molecules on its creases and folds when transferred onto diamond. The hydrophobicities of diamond and graphene stimulate instability of the planar water interface, and the fluctuations of these interfaces can destabilize and expel liquid, leading to spontaneous cavitation. At the spots where water molecules were expelled, graphene adheres strongly to diamond by capillary adhesion and traps the clustered water molecules in between. Further heating of the graphene-diamond promotes bonding between sp^2 graphene and sp^3 diamond and seal pockets of water molecules within the nanocavities.

Apart from water, other solvents can also be entrapped when graphene floats on them. For example, the organic solvent carbon disulfide (CS_2), which has good solubility for polyphenyls, was selected. Its IR transparency makes it a suitable solvent for in situ FTIR studies. The disparity in the density and sizes of the GNBs produced in different liquids is due to the difference in surface tension, with a higher surface tension leading to finer corrugation of the graphene.[5] The polarity index k' of water and CS_2 is 9.0 and 1.0, respectively. After annealing the graphene–diamond interface at 1275 K for 45 min in ultrahigh vacuum, the GNBs formed by encapsulating CS_2 has a density of about 5×10^{10} cm^{-2}, while GNBs formed by water is 1.6 times denser (Figure 1). CS_2-encapsulated GNBs are on average 5 nm larger in diameter than water-encapsulated GNBs. As the internal pressure of the bubbles is dependent on the physical dimensions of the bubbles, it is expected that the internal pressure will vary according to the size of the bubbles. It should be noted that the majority of bubbles are measured to

[*] C. H. Y. X. Lim, Prof. K. P. Loh
Graphene Research Centre, Department of Chemistry
National University of Singapore
3 Science Drive 3, Singapore 117543 (Singapore)
E-mail: chmlohkp@nus.edu.sg
C. H. Y. X. Lim
NUS Graduate School for Integrative Sciences and Engineering
Centre for Life Sciences #05-01
28 Medical Drive, Singapore 117456 (Singapore)
M. Nesladek
IMOMEC, Hasselt University
Wetenschapspark, B 3590 Dipenbeek (Belgium)

[**] K.P.L. acknowledges MOE Tier II grant "From in situ observation to growth scaling of graphene quantum dots (R-143-000-493-112)".

Supporting information for this article is available on the WWW under http://dx.doi.org/10.1002/anie.201308682.

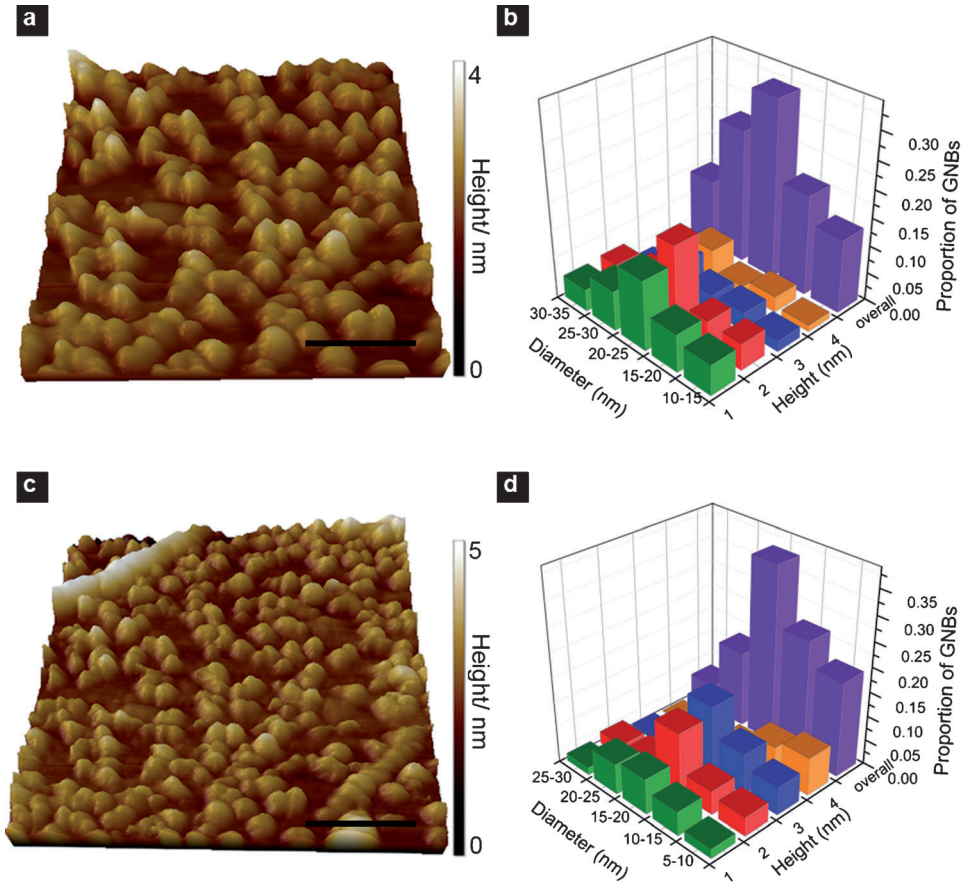

Figure 1. a), c) High-resolution three-dimensional topography representation of GNBs on diamond entrapping fluids, such as a) CS_2 and c) water. Scale bar: 100 nm. b) d) Histogram of the diameter and height distribution of GNBs entrapping b) CS_2 and d) water.

fall within 20–30 nm (diameters), thus the overall spectrum obtained is a collective signal, where the majority contribution to the resultant signal is from these bubbles. The presence of the trapped solvent can be detected by FTIR, even after annealing to temperatures where free solvent is expected to vaporize (Supporting Information, Figure S3).

The GNB-on-diamond, which entrapped the biphenyl molecules together with the solvent CS_2, was introduced into a Fourier-transform IR (FTIR) cell evacuated to 1×10^{-4} Torr. FTIR measurements conducted at room temperature using the cell reveal the intrinsic three-phonon absorption peaks of diamond,[6] together with the vibrational bands associated with the twisted conformation of biphenyl molecules (Figure 2a). It must be pointed out that in the absence of the graphene overlayer, any fluid that was introduced onto the diamond surface will evaporate readily in vacuum, which is in accordance with the inertness of the diamond surface. Thus the vibrational bands of the liquid can only be observed when it is trapped at the interface between diamond and graphene. The conformation of the biphenyl molecule is a result of the balance between the electrostatic repulsion of hydrogen atoms, which tends to twist the rings, and the interaction between π electrons, which tends to planarize the molecule.[7] We observed the disappearance of some peaks (indicated by arrows) in Figure 2b when the sample was heated to 373 K and beyond, these peaks correspond to the out-of-plane motion of hydrogen atoms. To obtain a rigorous basis for these observations, group theory was applied to account for the disappearance of certain vibrational modes. Representations of the biphenyl molecule in its twisted and planar form are shown in the Supporting Information, Figure S1. The twisted conformation of biphenyl belongs to the D_2 point group, and the vibrational modes can be classified as follows:

$$\Gamma = 15\,A \oplus 13\,B_1 \oplus 16\,B_2 \oplus 16\,B_3.$$

Modes belonging to the B_1, B_2, or B_3 irreducible representations are IR-active, for a total of 45 IR-active modes. For the planar configuration, biphenyl belongs to the D_{2h} point group and the vibrational modes are given by:

$$\Gamma = 11\,A_g \oplus 4\,A_u \oplus 3\,B_{1g} \oplus 10\,B_{2g} \oplus 6\,B_{3g} \oplus 10\,B_{1u} \oplus 6\,B_{2u} \oplus 10\,B_{3u}.$$

Modes belonging to the B_{1u}, B_{2u}, or B_{3u} irreducible representations are IR-active, for a total of 26 IR-active modes. Upon planarization, some of the B_1, B_2, and B_3 modes transform into B_{1g}, B_{2g}, and B_{3g} modes. These modes become IR-inactive as the dipole moment vectors exactly cancel each other. The disappearance of these IR peaks was echoed in a report by Zhuravlev et al.,[8] who studied the IR spectra of biphenyl under hydrostatic pressure using a piston-cylinder diamond-anvil cell.[9] Disappearance of similar IR peaks was observed at 0.18 GPa with the phase transition of biphenyl.[8,10] Thus, it can be inferred that the pressure in the GNB has reached the critical pressure of biphenyl when heated to 373 K. The temperature-dependent shifts of several out-of-plane hydrogen bending modes are plotted for the biphenyl molecule in Figure 2c. The blue-shifting of the out-of-plane modes at higher temperature indicates the shortening of intramolecular C–H bond and the increase in pressure in the GNB. As the critical pressure at which polyphenyls flatten increases with the number of phenyl rings, *p*-terphenyl and quarterphenyl were employed to extend the pressure range that can be determined. The flattening of *p*-terphenyl and quarterphenyl was reported to be observed at about 0.5 GPa and 1.0 GPa, respectively.[11] The disappearance of the specific IR peaks was observed at 473 K and 623 K for *p*-terphenyl and quarterphenyl, respectively, this allows us to derive the pressure-temperature relationship curve as depicted in Figure 2d.

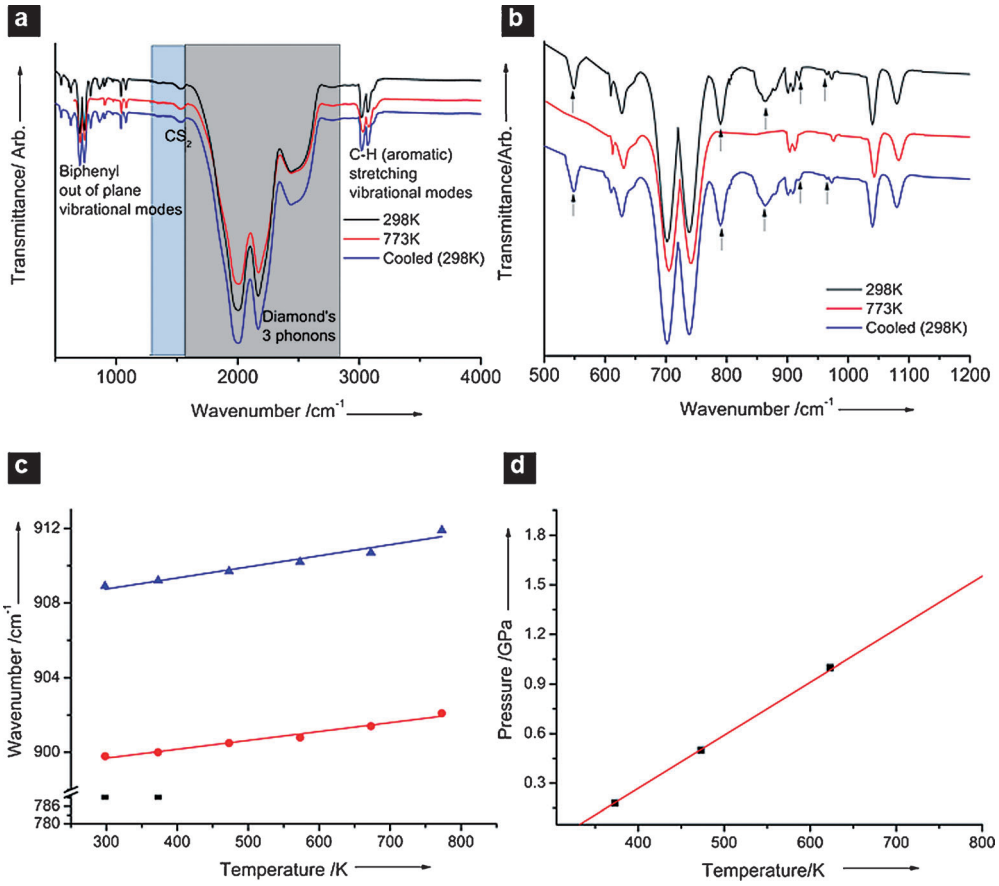

Figure 2. a) FTIR wide spectra of biphenyl in GNB on diamond before and after phase transition at 298 K, 773 K, and cooled to 298 K. b) Zoomed-in FTIR spectra showing out-of-plane modes of biphenyl in GNB on diamond before and after phase transition at 298 K, 773 K, and cooled to 298 K; c) frequency shifts of three biphenyl vibrational modes as a function of temperature. d) Pressure–temperature correlation.

To evaluate whether the pressure inside the bubble is effective for driving symmetry-forbidden reaction, we consider the [2+2] cycloaddition of C_{60} molecules. The oligomerization or of C_{60} is a model reaction for testing the pressure inside the GNB, as the progressive stages of coupling, from dimerization to trimerization and so on, exhibit well-defined pressure–temperature (*P*–*T*) phase boundaries. The [2+2] cycloaddition C_{60} is not favorable under normal conditions owing to the mismatch of molecular orbitals. However, this reaction can be activated photochemically via triplet excited states.[12] Polymerization of C_{60} has also been obtained by irradiation with electrons or ions,[13] plasma treatment,[13] alkali-metal doping,[14] direct chemical synthesis,[15] and even mechanical milling.[16] Finally, pressure can be used to compress C_{60} molecules and to drive intermolecular coupling.

The molecular nature of C_{60} molecule is apparent in its exceptionally simple vibrational spectrum, which exhibits four sharp IR modes, as expected for an isolated cage of icosahedral symmetry (Figure 3b (I)).[17] These vibrational properties change dramatically when the weak van der Waals forces among the fullerene molecules are replaced by covalent bonds.[12a,18] Formation of intercage covalent bonds reduces the molecular symmetry and gives rise to pronounced changes in the vibrational spectra.[19] The lowering of symmetry activate the silent I_h modes of C_{60} to result in appropriate splitting of the degenerate T_{1u} and H_g vibrational modes, giving rise to new bands at different stages of the polymerization.[18,20] The IR spectra in Figure 3b illustrate the phase transformations of C_{60} in GNB under various *P*–*T* windows. According to group theory, more than 300 modes in the $(C_{60})_2$ dimer (D) molecule and 150 vibrations of the distorted C_{60} cage in the orthorhombic (O) and tetragonal (T) polymers are predicted to exist in the IR and Raman spectra.[19a] However, experimentally observed IR and Raman spectra consist of only tens of well-distinguished bands owing to the low intensity of the certain vibration modes. As shown in Figure 3, the vibrational bands become more complex as the GNBs are heated, suggesting that phase transformation of C_{60} is occurring under heat and pressure. Features characteristic of pressure-polymerized forms of C_{60} are observed in the 600–700 cm^{-1} spectra region. The strong blue shifted bands at 615 (D), 605 (O), and 609 (T), which originate from the H_u (2) parent mode, is a clear indication of the modification of the fullerene cage. Several fingerprint bands due to individual distinct oligomer are observed. In the spectra of the dimer, the moderate band at 770 cm^{-1} and the sharp line at 762 cm^{-1} correspond to the activation of H_g (4) and F_{2g} (2) icosahedral even modes, respectively. The presence of a unique 1464 cm^{-1} band in the spectrum of the dimer (Figure 3b (II)) assignable to the A_g (2) derivative is a clear indication of the loss of inversion center by the C_{60} moiety. Furthermore, the peak at 1422 cm^{-1} with medium intensity can also be also used to identify $(C_{60})_2$ dimer from other polymeric forms.[21] The F_{2u} (2) mode in the polymeric species splits into doublets (711/716 cm^{-1} in the O and 709/719 cm^{-1} in T phases) with different relative intensities. Apart from the G_u (2) mode triplet splitting (730/741/747 cm^{-1}) in the spectra of tetragonal polymers, we also observed strong narrow lines at 759 (O) and 762 (T), which originate from the G_u (3) mode of C_{60}. The doublet residing at 608, 557 cm^{-1} and the downshifting of the pristine F_{1u} (1) mode from 527 to 523 cm^{-1} matches well with the value reported in a spectroscopic study of pressure modified C_{60}.[22] A sharp band at

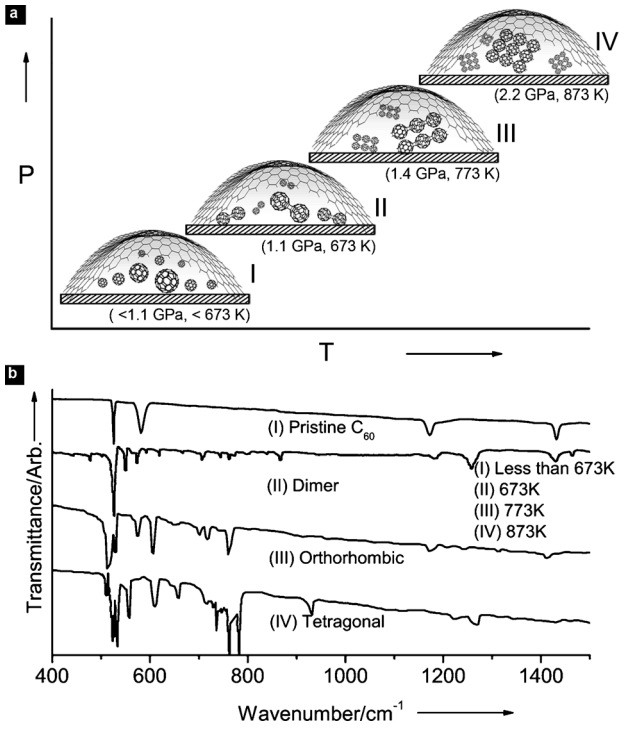

Figure 3. Structures showing the oligomerization of C_{60} inside GNB at different pressure–temperature windows a) (I) pristine C_{60}, (II) dimerization, (III) orthorhombic structure owing to the formation of trimer chains; (IV) tetragonal structure owing to 4 C_{60} molecules bonding in a square shape conformation. b) IR spectra of pristine, dimer, orthorhombic, and tetragonal phases of C_{60} (top to bottom).

932 cm^{-1} is observed in the fingerprint region of the tetragonal phase when the sample is heated to 873 K; it can thus be inferred that a sharp phase transition has occurred at this temperature. It is noteworthy to mention that the oligomerization reaction of C_{60} is irreversible, the distinctive spectroscopic signatures of the oliogomerized phases remained even after the samples were cooled to room temperature.

In summary, we have shown that GNB can be used as a bench-top anvil for the investigation of high pressure chemistry. The advantage of using the graphene–diamond hydrothermal anvil cell is that pressure is exerted isotropically on the sample, whereas in conventional cells, the axial force of the squeezer tends to deform the sample of interest. The anisotropy of some crystals and carbon phases obtained from C_{60} fullerite under high pressure has been attributed to the additional pressure component that occurs in the quasi-hydrostatic experimental conditions in the conventional anvil cell.[23,24] Owing to the transparency of graphene, it should be possible to study photochemical reactions in the trapped fluids by directing lasers on the GNB. Finally, such graphene bubbles can be used as adaptive focus lenses by combining the approaches of the fluidic lens and liquid-crystal lens. The change in curvature of the bubbles induced by expanding liquid can result in focal length changes owing to changes in refractive indexes, which can be deployed in optical bistability-based control schemes.

Experimental Section

The graphene sheets used in this study were grown by CVD following previous reported procedures.[25] The process was carried out in a quartz tube at reduced pressure with copper as a catalyst for graphene growth. The copper foil (thickness of 25 μm, purity of 99.8 %) was heated at 1275 K under a 10 sccm flow of H_2 (ca. 400 mTorr) to reduce the oxide present, increase the grain size, and ensure a smooth surface for growth. Next, CH_4 was introduced into the chamber for growth. CH_4 (10 sccm) and H_2 (10 sccm) were maintained at about 750 mTorr for 30 min. Following that, the grown sheet was cooled in an atmosphere of H_2 to room temperature. The graphene on copper foil samples were coated with poly(methyl methacrylate) (PMMA) and transferred onto diamond substrates.

Type IIa CVD single-crystal diamonds (100) were purchased from Element Six and mechanically polished to give a root mean square of less than about 0.2 nm before use. Acid cleaning and hydrogen plasma cleaning of diamond were used for all of the diamond samples. Metallic impurities were first dissolved in hot aqua regia (HNO_3/HCl 1:3), followed by removing organic impurities from the diamond samples by hot "piranha" solution (H_2O_2/H_2SO_4 1:3) at 375 K for 1 h. Hydrogen termination of diamond samples was performed by microwave hydrogen-plasma treatment using 800 W microwave power and 300 sccm of hydrogen gas flow for 15 min.

The graphene-on-diamond samples were mounted on a Mo sample plate, transferred into a ultrahigh vacuum chamber with a base pressure of $< 10^{-10}$ Torr. Annealing was conducted at 1275 K for 45 min by e-beam heating (SPECS GmbH, Germany). Throughout the entire annealing process, it was ensured that the pressure did not rise beyond 10^{-8} Torr.

A Dimension ICO using a Nanoscope V controller (Bruker, Santa Barbra, CA) equipped with a diamond probe (DNISP; Bruker AFM Probes, Camarillo, CA) was operated in Peakforce Quantitative Nanomechanical mode for simultaneous topography imaging and Young's modulus mapping of the graphene bubbles.

FTIR measurements were conducted in the reflection mode using an OPUS/IR PS15 spectrometer (Bruker). The sample was loaded into a high-temperature high-pressure FTIR cell evacuated to 1×10^{-4} Torr. The spectra were the results of 32 co-added interferograms at 4 cm^{-1} resolution between 400 to 4000 cm^{-1} with collection times of approximately 2 min. Each sample was analyzed at least three times to ensure the reproducibility of the results.

Received: October 5, 2013
Published online: November 20, 2013

Keywords: anvil cells · conformational changes · diamond · graphene · high pressure

[1] C. Lee, X. Wei, J. W. Kysar, J. Hone, *Science* **2008**, *321*, 385 – 388.
[2] J. M. Yuk, J. W. Park, P. Ercius, M. F. Crommie, A. Zettl, A. P. Alivisatos, *Science* **2012**, *336*, 61 – 64.
[3] C. H. Y. X. Lim, A. Sorkin, Q. Bao, A. Li, K. Zhang, M. Nesladek, K. P. Loh, *Nat. Commun.* **2013**, *4*, 1556.
[4] R. A. Forman, G. J. Piermarini, J. D. Barnett, S. Block, *Science* **1972**, *176*, 284 – 285.
[5] Y. Pomeranz, C. E. Meloan, *Food Analysis*: *Theory and Practice*, Aspen Publishers, Gaithersburg, **2000**.
[6] S. J. Charles, J. E. Butler, B. N. Feygelson, M. E. Newton, D. L. Carroll, J. W. Steeds, H. Darwish, C. S. Yan, H. K. Mao, R. J. Hemley, *Phys. Status Solidi A* **2004**, *201*, 2473 – 2485.
[7] a) D. Cremer, *Tetrahedron* **1988**, *44*, 7427 – 7454; b) I. Fischer-Hjalmars, *Tetrahedron* **1963**, *19*, 1805 – 1815.
[8] K. K. Zhuravlev, M. D. McCluskey, *J. Chem. Phys.* **2002**, *117*, 3748 – 3752.

[9] G. Yu. Machavariani, M. P. Pasternak, G. R. Hearne, G. K. Rozenberg, *Rev. Sci. Instrum.* **1998**, *69*, 1423 – 1425.
[10] M. H. Lemée-Cailleau, A. Girard, H. Cailleau, Y. Délugeard, *Phys. Rev. B* **1992**, *45*, 12682 – 12690.
[11] a) B. J. Baer, E. L. Chronister, *J. Chem. Phys.* **1993**, *99*, 3137 – 3138; b) K. K. Zhuravlev, M. D. McCluskey, *J. Chem. Phys.* **2001**, *114*, 5465 – 5467.
[12] a) A. M. Rao, P. Zhou, K. A. Wang, G. T. Hager, J. M. Holden, Y. Wang, W. T. Lee, X. X. Bi, P. C. Eklund, D. S. Cornett, M. A. Duncan, I. J. Amster, *Science* **1993**, *259*, 955 – 957; b) A. M. Rao, M. Menon, K.-A. Wang, P. C. Eklund, K. R. Subbaswamy, D. S. Cornett, M. A. Duncan, I. J. Amster, *Chem. Phys. Lett.* **1994**, *224*, 106 – 112; c) P. Zhou, Z.-H. Dong, A. M. Rao, P. C. Eklund, *Chem. Phys. Lett.* **1993**, *211*, 337 – 340.
[13] B. Sundqvist in *Fullerene-Based Materials*, *Vol. 109* (Ed.: K. Prassides), Springer, Berlin/Heidelberg, **2004**, pp. 85 – 126.
[14] a) P. W. Stephens, G. Bortel, G. Falgel, M. Tegze, A. Janossy, S. Pekker, G. Oszlanyi, L. Forro, *Nature* **1994**, *370*, 636 – 639; b) B. Renker, H. Schober, M. Braden, *Solid State Commun.* **1999**, *109*, 423 – 426.
[15] G. W. Wang, K. Komatsu, Y. Murata, M. Shiro, *Nature* **1997**, *387*, 583 – 586.
[16] Z. G. Liu, H. Ohi, K. Tsuchiya, M. Umemoto, K. Masuyama, *J. Mater. Sci. Technol.* **1999**, *15*, 405 – 409.
[17] a) W. Krätschmer, K. Fostiropoulos, D. R. Huffman, *Chem. Phys. Lett.* **1990**, *170*, 167 – 170; b) M. S. Dresselhaus, G. Dresselhaus, P. C. Eklund, *Science of fullerenes and carbon nanotubes* [electronic resource], Academic Press, San Diego, **1996**.
[18] Y. Iwasa, T. Arima, R. M. Fleming, T. Siegrist, O. Zhou, R. C. Haddon, L. J. Rothberg, K. B. Lyons, H. L. Carter, Jr., A. F. Hebard, R. Tycko, G. Dabbagh, J. J. Krajewski, G. A. Thomas, T. Yagi, *Science* **1994**, *264*, 1570 – 1572.
[19] a) V. A. Davydov, L. S. Kashevarova, A. V. Rakhmanina, V. M. Senyavin, R. Céolin, H. Szwarc, H. Allouchi, V. Agafonov, *Phys. Rev. B* **2000**, *61*, 11936 – 11945; b) M. C. Martin, D. Koller, X. Du, P. W. Stephens, L. Mihaly, *Phys. Rev. B* **1994**, *49*, 10818 – 10821.
[20] a) C. H. Xu, G. E. Scuseria, *Phys. Rev. Lett.* **1995**, *74*, 274 – 277; b) K. Komatsu, G. W. Wang, Y. Murata, T. Tanaka, K. Fujiwara, K. Yamamoto, M. Saunders, *J. Org. Chem.* **1998**, *63*, 9358 – 9366; c) S. Lebedkin, A. Gromov, S. Giesa, R. Gleiter, B. Renker, H. Rietschel, W. Krätschmer, *Chem. Phys. Lett.* **1998**, *285*, 210 – 215.
[21] S. G. Stepanian, V. A. Karachevtsev, A. M. Plokhotnichenko, L. Adamowicz, A. M. Rao, *J. Phys. Chem. B* **2006**, *110*, 15769 – 15775.
[22] M. E. Kozlov, M. Tokumoto, K. Yakushi, *Appl. Phys. A* **1997**, *64*, 241 – 245.
[23] M. Núñez-Regueiro, L. Marques, J. L. Hodeau, *The Physics of Fullerene-Based and Fullerene-Related Materials*, *Vol. 23* (Ed.: W. Andreoni), Kluwer Academic Publishers, Dordrecht, **2000**.
[24] A. G. Glazov, V. V. Mukhamad′yarov, V. V. Brazhkin, A. G. Lyapin, E. L. Gromnitskaya, O. V. Stal′gorova, S. V. Popova, *JETP Lett.* **2001**, *73*, 552 – 556.
[25] X. Li, W. Cai, J. An, S. Kim, J. Nah, D. Yang, R. Piner, A. Velamakanni, I. Jung, E. Tutuc, S. K. Banerjee, L. Colombo, R. S. Ruoff, *Science* **2009**, *324*, 1312 – 1314.

